20th AIAA Computational Fluid Dynamics Conference
27 - 30 June 2011, Honolulu, Hawaii

AIAA 2011-3401

Numerical Prediction of Three-Dimensional Non-Equilibrium Gaseous Flows Using the Gaussian Moment Closure

C. K. S. Lam* and C. P. T. Groth†

University of Toronto Institute for Aerospace Studies

4925 Dufferin Street, Toronto, Ontario, Canada, M3H 5T6

A parallel, implicit, adaptive mesh refinement (AMR), upwind, finite-volume scheme is described for the solution of the 10-moment Gaussian closure and the combined hyperbolic modelling treatment / numerical method is applied to the prediction of three-dimensional, non-equilibrium, micro-scale, gaseous flows. The Gaussian moment equations are based on a maximum-entropy closure applied to the Boltzmann equation and provides a fully-realisable and strictly hyperbolic description of non-equilibrium gaseous flows that is valid from the near-equilibrium or continuum limit, through the transition regime, up to the near-collisionless or free-molecular flow limit. Although this somewhat simplified mathematical model does not incorporate the effects of heat transfer, it has been shown to accurately describe non-equilibrium momentum transport for a range of micro-scale flows and is very representative of other higher-order closures that would potentially include the effects of non-equilibrium thermal transport. The hyperbolic moment equations are readily amenable to solutions using a Godunov-type, upwind, finite-volume scheme on an AMR mesh. The proposed upwind scheme makes use of Riemann-solver-based flux functions and limited linear reconstruction to provide accurate and monotonic solutions, even in the presence of large solution gradients and/or under-resolved solution content on three-dimensional, multi-block, body-fitted, hexahedral mesh. A block-based AMR strategy is adopted herein to allow for local refinement of the computational mesh. A rather effective and scalable parallel implicit time-marching scheme based on a Jacobian-free inexact Newton-Krylov-Schwarz (NKS) approach with additive Schwarz preconditioning and domain partitioning following from the multi-block AMR mesh is used for the solution of the non-linear ordinary-differential equations that result from the application of the upwind spatial discretisation procedure. Details are given of the Gaussian closure, along with suitable extensions for diatomic gases and slip-flow boundaries, and the proposed finite-volume method. Numerical results for several canonical flow problems demonstrate the potential of hyperbolic moment closures, combined with an efficient parallel solution method, for accurately predicting fully three-dimensional non-equilibrium gaseous flow behaviour.

I. Introduction

A. Transition-Regime Micro-Scale Flows

Gaseous flow behaviour is commonly described in computational fluid dynamics (CFD) through the Navier-Stokes equations. This mathematical description has proven to be useful in describing fluid flow in problems frequently encountered in aerospace engineering. For such problems, the discrete nature of the particles making up the gas is ignored and the gas is treated in a continuous manner, with intermolecular collisions occurring frequently enough to warrant this near-equilibrium assumption. At the other end of the dimensional spectrum, the treatment of highly-rarefied gaseous flows in the near-collisionless limit requires a microscopic treatment as offered by particle simulation techniques such as the Direct Simulation Monte Carlo (DSMC) developed by Bird.[1] While DSMC techniques are valid for the full range of flow regimes from the continuum

*P. h. D. Student, Email:lam@utias.utoronto.ca

†Professor, Email:groth@utias.utias.utoronto.ca, Senior Member AIAA

to the free-molecular-flow limits, the computational expenses required increase dramatically as the near-equilibrium limit is approached as more simulation particles are needed.

In general, the regimes for gaseous flows can be characterised by the non-dimensional Knudsen number, $Kn = \frac{\lambda}{L}$, where λ is the mean free path between interparticle collisions and L is the characteristic length scale of the problem of interest. Continuum-limit flows are dominated by interparticle collisions with very short mean free paths, with Knudsen numbers in the range $Kn < 0.01$. Conversely, non-equilibrium flows can occur due to low gas densities creating large mean free paths (as in rarefied flows) or for very small length scales where particle collisions are infrequent. In both of these cases, the Knudsen number exceeds 0.01 and becomes large as the deviation from equilibrium conditions becomes significant. The collisionless regime is taken to occur for $Kn > 10 - 100$. Recent scientific technologies using micro-electromechanical systems (MEMS) occur in flow regimes that occupy a transitional regime between the two extremes, the continuum and collisionless limits, with $0.01 < Kn < 10 - 100$. In this transitional regime, the conventional fluid dynamic description offered by the Navier-Stokes equations will generally fail, yet the number of particles required can still make particle simulation methods impractical. This is obviously problematic and development of improved mathematical models and numerical methods for treating this transitional regime, with an economical extension for the continuum flow regime, would not only be invaluable for improving our understanding of non-equilibrium flow physics, but would also greatly aid in the design and development of micro-scale technologies.

B. Moment Closures

The use of moment methods for non-equilibrium gases was first hypothesised by Maxwell.[2] Later, Boltzmann provided a means with which to study the evolution of these distribution functions, which in turn gave transport equations for various macroscopic properties.[3] However, the construction of the resulting moment equations is such that each transport equation relies on the flux of a higher-order velocity moment *ad infinitum*. One approach to closing off this set of equations for practical purposes is to assume a particular form for the non-equilibrium distribution function having a fixed number of free parameters in such a way that the higher-order closing velocity moment can be expressed solely in terms of lower ones. Grad[4] considered moment closures based on a truncated polynomial power series expansion for the approximate distribution function and this technique generated first-order systems of hyperbolic partial differential equations (PDEs) describing the time evolution of the macroscopic moments. However, hyperbolicity of the Grad moment equations is not guaranteed for all flow conditions and leads to closure breakdown. The assumed form of the distribution function is also not always physically plausible.

An alternative hierarchy of maximum-entropy moment closures has been developed by Levermore.[5] The Levermore hierarchy has a number of desirable mathematical properties including strict hyperbolicity, thus the possibility of closure breakdown in this sense is avoided. The lowest order of this hierarchy of closures is the 5-moment closure that corresponds to the Euler equations, while the next member results in the 10-moment closure, also known as the Gaussian closure. While a full guarantee of hyperbolicity applies only to these two lowest-order closures in the hierarchy,[6] the usefulness of the 10-moment Gaussian closure is evident from a computational standpoint. Being purely hyperbolic with only first-order derivatives, the solution is guaranteed to have finite speeds of propagation. Moreover, numerical solutions can be readily obtained using the highly successful class of Godunov-type finite volume schemes developed for hyperbolic conservation laws without excessive modification.[7] These schemes are robust, accurate, and can preserve the conservation properties of the solution at the discrete level. They can also be applied using a large variety of boundary conditions and meshing techniques and, for first-order systems, provide solutions that are generally rather insensitive to irregularities in the mesh.

The Gaussian closure is a somewhat simplified mathematical model as it does not incorporate the effects of heat transfer. Nevertheless, it has been shown to accurately describe non-equilibrium momentum transport for a range of micro-scale flows and is very representative of other higher-order closures that would potentially include the effects of non-equilibrium thermal transport.[8–10] The numerical solution and application of the Gaussian closure for two-dimensional micro-scale flows has been studied extensively by McDonald and Groth,[8–10] with considerations for diatomic gases following the approach devised by Hittinger[11] as well as with a regularisation correction for heat transfer effects.[9]

C. Scope of this Study

In this study, the extension of the previous two-dimensional work by McDonald and Groth[8–10] to the three-dimensional flow case is considered. A parallel, fully-implicit, adaptive mesh refinement (AMR), upwind, finite-volume scheme is described for the solution of the 10-moment Gaussian closure and the combined hyperbolic modelling treatment / numerical method is applied to the prediction of three-dimensional, non-equilibrium, micro-scale, gaseous flows. As in the previous studies, the proposed upwind scheme makes use of Riemann-solver-based flux functions and limited linear reconstruction to provide accurate and monotonic solutions, even in the presence of large solution gradients and/or under-resolved solution content on three-dimensional, multi-block, body-fitted, hexahedral mesh. A block-based AMR strategy is used here to allow for local refinement of the computational mesh based on the procedure of Gao and Groth.[12–14] Unlike the previous two-dimensional studies where a semi-implicit time-marching method was utilised, a rather effective and scalable parallel implicit time-marching scheme based on a Jacobian-free inexact Newton-Krylov-Schwarz (NKS) approach with additive Schwarz preconditioning and domain partitioning following from the multi-block AMR mesh is used here for the solution of the non-linear ordinary-differential equations that result from the application of the upwind spatial discretisation procedure.[15–17] Details are given of the Gaussian closure, along with suitable extensions for diatomic gases and slip-flow boundaries, and the proposed finite-volume method. Numerical results for several canonical flow problems demonstrate the potential of hyperbolic moment closures, combined with an efficient parallel solution method, for accurately predicting fully three-dimensional non-equilibrium gaseous flow behaviour.

II. Governing Equations

A. Kinetic Theory and Phase Space Distribution Function

The kinetic theory of gases treats fluids as a collection of minute particles, interacting with each other and its external container through collisions to create macroscopic properties such as density and pressure. The transfer of energy between particles through the collisions can be solely described through classical mechanics obeying Newton's laws of motion. However, constructing a set of equations in this manner for each particle in a fluid along with its associated collisional processes is highly impractical considering the large number of particles present in even the most rarefied gases.

Kinetic theory instead relies on a statistical description of fluid particles based on its spatial location, x_i, and its velocity, v_i, at a particular moment in time, t. As particle position and velocity are independent of each other in the absence of external forces, a complete statistical description of the gaseous particles can be provided by a six-dimensional phase space distribution function spanning three-dimensional physical space and velocity space. The resulting description yields a probability density function, $F(x_i, v_i, t)$, that describes the number of particles occupying an elemental volume in physical space and velocity space at a point in time.

B. Maxwell-Boltzmann Distribution and the Boltzmann Equation

For a monatomic gas in thermal equilibrium, a mathematical description of the phase-space distribution function was first established by Maxwell[2] and subsequently expanded and developed by Boltzmann,[18] and is known today as the the Maxwell-Boltzmann distribution function, M, given by

$$M(\vec{v}) = n\left(\frac{m}{2\pi kT}\right)^{\frac{3}{2}} e^{-\frac{mv^2}{2kT}}, \tag{1}$$

where $\vec{v}$ is the velocity vector, m is the mass, T is the temperature, and k is the Boltzmann constant.

In the general non-equilibrium case, the form of phase-space distribution function can vary widely; however, the time evolution of the distribution function is always described as a function of time and the six-dimensional phase space through the non-linear, integro-differential, kinetic equation referred to as the Boltzmann equation and given by

$$\frac{\partial F}{\partial t} + v_i\frac{\partial F}{\partial x_i} + a_i\frac{\partial F}{\partial v_i} = \frac{\delta F}{\delta t}, \tag{2}$$

where here F is any general non-equilibrium distribution function, $\frac{\delta F}{\delta t}$ represents the rate of change of the distribution function due to collisions (this term involves the evaluation of a five-dimensional integral

expression), and x_i, v_i, a_i are the physical space, velocity and acceleration vectors, respectively. It can be shown that the Maxwell-Boltzmann distribution function is the equilibrium solution of the Boltzmann equation with no applied external forces ($a_i = 0$).

C. Macroscopic Properties and Maxwell's Equation of Change

Within the statistical description offered by kinetic theory, macroscopic properties of the gas are essentially expected values of functionals of velocity space, $W(\vec{v})$, and can be found by multiplying these functionals with the probability distribution and integrating over velocity space as follows

$$\psi = m \langle W(\vec{v})F \rangle = m \iiint_{\infty} W(\vec{v})F d\vec{v}, \tag{3}$$

where ψ is the macroscopic property of interest. Having defined the macroscopic property, the Boltzmann equation also provides a description of the time evolution of the macroscopic moments, and thus their transport behaviour. Moment equations describing the transport of the macroscopic quantities can be obtained by weighting the Boltzmann equation and integrating term by term. Neglecting external forces, the resulting moment equations arising from the Boltzmann equation, Maxwell's equation of change, can be written as

$$\psi = \psi(\vec{x}, t) = \psi \frac{\partial}{\partial t}(m \langle W(\vec{v})F \rangle) + \frac{\partial}{\partial x_i}(m \langle v_i W(\vec{v})F \rangle) = \Delta \left[mW(\vec{v})F \right], \tag{4}$$

$$\Delta \left[mW(\vec{v})F \right] = m \iiint_{\infty} W(\vec{v}) \frac{\delta F}{\delta t} d\vec{v} \tag{5}$$

where $\Delta \left[mW(\vec{v})F \right]$ represents the production and destruction of the moment produced by interparticle collisions. This collision term assumes that only binary collisions occur, as the probability of collisions involving more than two collision partners at exactly the same instance in time and space are rare and will not contribute significantly to the transport of macroscopic properties. At this point, it is important to note that the evaluation of each moment equation requires the evaluation of its flux or the next higher-order velocity moment. This means that the exact representation of the evolution of the distribution function requires the evaluation of an infinite set of coupled moment equations.

D. Moment Methods

As noted above, the Boltzmann equation (2) in its original form is a non-linear, integro-differential equation with seven independent variables in time, physical space and velocity space. The complexity in solving this equation or its resultant infinite set of coupled moment equations in non-trivial cases has led to the use of approximate solution methods for the Boltzmann equation based on the stipulation of a specific form of the distribution function and approximate expressions for the collision term. The approximate form of the distribution function results in a closing expression for the moment equations. A brief summary of moment closure techniques and the Gaussian closure now follows.

1. Relaxation-Time Approximation for Collision Operator

The five-dimensional integral expression for the exact collision term appearing in the Boltzmann equation above is frequently approximated by the Bhatnagar-Gross-Krook (BGK) or relaxation time approximation.[19] In this mathematical simplification, the collision term is replaced by the expression

$$\frac{\delta F}{\delta t} = -\frac{F - M}{\tau}, \tag{6}$$

where F is a general phase space distribution, M is the local Maxwell-Boltzmann distribution function reached at equilibrium, where both F and M share the same moments, and τ is a relaxation time representative of the collisional processes. While the BGK approximation is a reasonable approximation, the use of a single time scale to describe the evolution of all the moments of the distribution function is a fundamental source of error since the diffusion of mass, momentum and energy in a real gas all occur at different time scales while approaching equilibrium conditions. This amounts to stating that the Prandtl number $\mathrm{Pr} = 1$

for these flows, as the relaxation time for the diffusion of momentum and internal energy is assumed equal. For systems with only small perturbations from equilibrium, the simplicity of the BGK approximation makes it an effective tool for modelling the behaviour of the distribution function[20] and it is therefore used herein.

2. 10-Moment Gaussian Closure

To resolve the problem of evaluating an infinite number of coupled moment equations, the distribution function can be assumed to have a particular form, where undetermined coefficients associated with this approximate form can be related to a set of velocity moments of interest. In doing so, the highest order moment of interest can be expressed as a function of a set of lower-order moments, thus providing closure for the equation set. In the Gaussian, maximum-entropy, moment closure of the Levermore hierarchy,[5] the distribution function is assumed to take the form

$$F \approx G(t, x_i, v_i) = \frac{\rho}{m(2\pi)^{\frac{3}{2}}(\det\boldsymbol{\Theta})^{\frac{1}{2}}} \exp\left(-\frac{1}{2}(\Theta_{ij})^{-1}c_i c_j\right), \tag{7}$$

where Θ is a symmetric tensor defined by $\Theta_{ij} = \frac{P_{ij}}{\rho}$, P_{ij} is the generalised pressure tensor and ρ is the density. The Gaussian distribution function G is a function of the density, velocity and generalised pressure tensor and these may be obtained by solving the set of moment equations arising from Maxwell's equation of change with $F = G$.

The moment equations of the Gaussian closure are equivalent to those arising from the Grad 10-moment closure,[4] and similarly do not take into account heat transfer, as the third-order velocity moments $\langle mc_i c_j c_k G\rangle$ reduce to zero. The resulting 10-moment equations in divergence form describing the transport of mass, momentum and bulk and random motion energy in each coordinate direction are given by

$$\frac{\partial\rho}{\partial t} + \frac{\partial}{\partial x_k}(\rho u_k) = 0, \tag{8}$$

$$\frac{\partial}{\partial t}(\rho u_i) + \frac{\partial}{\partial x_k}(\rho u_i u_k + P_{ik}) = 0, \tag{9}$$

$$\frac{\partial}{\partial t}(\rho u_i u_j + P_{ij}) + \frac{\partial}{\partial x_k}(\rho u_i u_j u_k + u_k P_{ij} + u_j P_{ik} + u_i P_{jk}) = -\frac{1}{\tau}(P_{ij} - \frac{1}{3}P_{kk}\delta_{ij}) \tag{10}$$

where where u_i is the bulk particle velocity, and the relaxation time approximation has been used in the evaluation of the collision terms appearing in the generalised energy tensor equation.

3. Solid Wall Boundary Conditions

A simple solid-wall boundary condition is employed for all of the flow problems considered in this paper. By assuming the existence of a Knudsen layer at the wall next to the solid surface, the particles at the surface can be described as a combination of the distribution functions of incoming and reflected particles. A fully diffuse reflection is assumed for the reflected particles. The moments of the resulting combination of distribution functions then provides the solid wall boundary conditions needed for the Gaussian closure. A similar approach for solid wall boundary conditions was used by McDonald and Groth in earlier studies of the Gaussian closure applied to two-dimensional micro-scale flows.[8–10]

E. Extension for Diatomic Gases

The construction of the transport equations for the Gaussian closure up to now have assumed that the gas is composed of monatomic particles with no internal degrees of freedom. The energy of rotational and vibrational modes are appropriately taken to be zero, as their contribution to the mechanics of relaxation towards complete equilibrium is negligible. Many practical flow applications, however, involve the use of diatomic particles such as nitrogen and oxygen. Although at modest temperatures the energy associated with vibrational modes of diatomic particles can still be neglected, the energy of the internal rotational modes is significant and must be accounted for.

For a diatomic particle, there are two rotational energy modes which, for this analysis, can be assumed to equal due to symmetry. The method used by Hittinger,[11] based on a simple rotational model for the diatomic molecule, is used here to account for rotational energy of these two modes. The BGK approximation for the

source terms is modified to account for an additional relaxation time associated with the rotational degrees of freedom, and takes the form

$$\frac{\delta G_D}{\delta t} = -\frac{G_D - F_D}{\tau_t} - \frac{F_D - M_D}{\tau_r} \tag{11}$$

where F_D and M_D represent an intermediate distribution function and the diatomic equilibrium Maxwell-Boltzmann distribution function respectively, and τ_r is a relaxation time associated the relaxation process for rotational equilibrium. This model states that the general non-equilibrium distribution function, G_D, relaxes to some intermediate distribution function, F_D, on a time scale, τ_t, whereupon equilibrium is achieved for the translational degrees of freedom, but not necessarily for the rotational degrees of freedom. A further relaxation process on a time scale, τ_r, moves this intermediate distribution function towards true equilibrium for all degrees of freedom described by the Maxwell-Boltzmann distribution function for a diatomic gas, M_D.

In three dimensions, an additional transport equation is added to the original set of ten to account for this rotational energy, and an additional relaxation term presents itself in the macroscopic energy density. The final set of eleven transport equations in divergence form are then as follows:

$$\frac{\partial \rho}{\partial t} + \frac{\partial}{\partial x_k}(\rho u_k) = 0, \tag{12}$$

$$\frac{\partial}{\partial t}(\rho u_i) + \frac{\partial}{\partial x_k}(\rho u_i u_k + P_{ik}) = 0, \tag{13}$$

$$\frac{\partial}{\partial t}(\rho u_i u_j + P_{ij}) + \frac{\partial}{\partial x_k}(\rho u_i u_j u_k + u_k P_{ij} + u_j P_{ik} + u_i P_{jk}) = -\frac{P_{ij} - \frac{1}{3}P_{kk}\delta_{ij}}{\tau_t} - \frac{\frac{1}{3}P_{kk}\delta_{ij} - p\delta_{ij}}{\tau_r}, \tag{14}$$

$$\frac{\partial E_{rot}}{\partial t} + \frac{\partial}{\partial x_k}(u_k E_{rot}) = -\frac{E_{rot} - p}{\tau_r} \tag{15}$$

where E_{rot} is the rotational energy, and p is the equilibrium isotropic pressure.

F. Eigenstructure

The eigenstructure of the Gaussian closure is of interest here not only because of its use in Riemann-solver based flux functions for the proposed Godunov-type finite volume schemes, but also to demonstrate the hyperbolicity of the system and the propagation characteristics of various macroscopic properties. Equations (12)-(15) can be written in weak conservation form as

$$\frac{\partial \mathbf{U}}{\partial t} + \frac{\partial \mathbf{E}}{\partial x} + \frac{\partial \mathbf{F}}{\partial y} + \frac{\partial \mathbf{G}}{\partial z} = \mathbf{S}, \tag{16}$$

where $\mathbf{U}$ is the vector of conserved variables, $\mathbf{S}$ is the source vector, and $\mathbf{E}$, $\mathbf{F}$, and $\mathbf{G}$ are the flux vectors in the x, y, and z directions respectively. The vectors are defined as

$$\mathbf{U} = \begin{bmatrix} \rho \\ \rho u \\ \rho v \\ \rho w \\ \rho u^2 + P_{xx} \\ \rho uv + P_{xy} \\ \rho uw + P_{xz} \\ \rho v^2 + P_{yy} \\ \rho vw + P_{yz} \\ \rho w^2 + P_{zz} \\ E_{rot} \end{bmatrix}, \quad \mathbf{E} = \begin{bmatrix} \rho u \\ \rho u^2 + P_{xx} \\ \rho uv + P_{xy} \\ \rho uw + P_{xz} \\ \rho u^3 + 3uP_{xx} \\ \rho u^2 v + 2uP_{xy} + vP_{xx} \\ \rho u^2 w + 2uP_{xz} + wP_{xx} \\ \rho uv^2 + uP_{yy} + 2vP_{xy} \\ \rho uvw + uP_{yz} + vP_{xz} + wP_{xy} \\ \rho w^2 u + uP_{zz} + 2wP_{xz} \\ uE_{rot} \end{bmatrix}, \quad \mathbf{F} = \begin{bmatrix} \rho v \\ \rho uv + P_{xy} \\ \rho v^2 + P_{yy} \\ \rho vw + P_{yz} \\ \rho u^2 v + 2uP_{xy} + vP_{xx} \\ \rho uv^2 + uP_{yy} + 2vP_{xy} \\ \rho uvw + uP_{yz} + vP_{xz} + wP_{xy} \\ \rho v^3 + 3vP_{yy} \\ \rho v^2 w + 2vP_{yz} + wP_{yy} \\ \rho vw^2 + vP_{zz} + 2wP_{yz} \\ vE_{rot} \end{bmatrix},$$

$$\mathbf{G} = \begin{bmatrix} \rho w \\ \rho uw + P_{xz} \\ \rho vw + P_{yz} \\ \rho w^2 + P_{zz} \\ \rho u^2 w + 2uP_{xz} + wP_{xx} \\ \rho uvw + uP_{yz} + vP_{xz} + wP_{xy} \\ \rho uw^2 + uP_{zz} + 2wP_{xz} \\ \rho v^2 w + 2vP_{yz} + wP_{yy} \\ \rho vw^2 + vP_{zz} + 2wP_{yz} \\ \rho w^3 + 3wP_{zz} \\ wE_{rot} \end{bmatrix}, \quad \mathbf{S} = \begin{bmatrix} 0 \\ 0 \\ 0 \\ 0 \\ -\frac{1}{3\tau_t}\left(2P_{xx} - P_{yy} - P_{zz}\right) - \frac{2}{15\tau_r}\left(P_{xx} + P_{yy} + P_{zz} - 3E_{rot}\right) \\ -\frac{P_{xy}}{\tau_t} \\ -\frac{P_{xz}}{\tau_t} \\ -\frac{1}{3\tau_t}\left(-P_{xx} + 2P_{yy} - P_{zz}\right) - \frac{2}{15\tau_r}\left(P_{xx} + P_{yy} + P_{zz} - 3E_{rot}\right) \\ -\frac{P_{yz}}{\tau_t} \\ -\frac{1}{3\tau_t}\left(-P_{xx} - P_{yy} + 2P_{zz}\right) - \frac{2}{15\tau_r}\left(P_{xx} + P_{yy} + P_{zz} - 3E_{rot}\right) \\ -\frac{1}{5\tau_r}\left(3E_{rot} - P_{xx} - P_{yy} - P_{zz}\right) \end{bmatrix}$$

To define the relaxation times for translational and rotational equilibrium, the bulk and dynamic viscosities for the fluid are used. In the near-equilibrium limit for perfect gases, rotational relaxation exhibits itself as a major source of of bulk viscosity. By using a perturbative expansion technique, Hittinger[11] has previously shown that the translational and rotational relaxation times can be related to the dynamic viscosity, μ, and the bulk viscosity, μ_B, through the relation

$$\tau_t \sim \frac{\mu}{p}, \quad \tau_r \sim \frac{15\mu_B}{4p}, \tag{17}$$

where p is the thermodynamic pressure.

The conservative form of Equations (16) can also be written with flux Jacobians as

$$\frac{\partial \mathbf{U}}{\partial t} + \mathbf{A}\frac{\partial \mathbf{U}}{\partial x} + \mathbf{B}\frac{\partial \mathbf{U}}{\partial y} + \mathbf{C}\frac{\partial \mathbf{U}}{\partial z} = \mathbf{S}, \tag{18}$$

where $\mathbf{A} = \frac{\partial \mathbf{F}}{\partial \mathbf{U}}$, $\mathbf{B} = \frac{\partial \mathbf{E}}{\partial \mathbf{U}}$, and $\mathbf{C} = \frac{\partial \mathbf{G}}{\partial \mathbf{U}}$.

When considering wave propagation or transport in the x-direction, the eigenvalues, λ_i, of the Jacobian matrix $\mathbf{A}$ in are found to be

$$\lambda_{1-11} = \left(u - \sqrt{3}c_{xx}, u - c_{xx}, u - c_{xx}, u, u, u, u, u, u + c_{xx}, u + c_{xx}, u + \sqrt{3}c_{xx}\right) \tag{19}$$

where $c_{xx} = \sqrt{\frac{P_{xx}}{\rho}}$ is representative of an x-directional 'sound' or 'acoustic' speed. These eigenvalues are representative of the propagation speeds of small disturbances for the Gaussian closure, and are all real when $\rho > 0$ and $P_{xx} > 0$. The right eigenvectors, $\mathbf{r_{ci}}$, show the hydrodynamic properties affected by each of these wave speeds and are written as

$$\mathbf{r_{c1}} = \begin{bmatrix} 1 \\ u - \sqrt{3}c_{xx} \\ v - \frac{\sqrt{3}P_{xy}}{c_{xx}\rho} \\ w - \frac{\sqrt{3}P_{xz}}{c_{xx}\rho} \\ 3c_{xx}^2 - 2\sqrt{3}uc_{xx} + u^2 \\ \frac{\rho uvc_{xx} - u\sqrt{3}P_{xy} - \sqrt{3}c_{xx}^2\rho v + 3c_{xx}P_{xy}}{c_{xx}\rho} \\ \frac{\rho uwc_{xx} - u\sqrt{3}P_{xz} - \sqrt{3}c_{xx}^2\rho w + 3c_{xx}P_{xz}}{c_{xx}\rho} \\ \frac{\rho^2 v^2 c_{xx}^2 - 2\sqrt{3}P_{xy}c_{xx}\rho v + \rho c_{xx}^2 P_{yy} + 2P_{xy}^2}{\rho^2 c_{xx}^2} \\ \frac{c_{xx}\rho\left(-\sqrt{3}(wP_{xy} + vP_{xz}) + c_{xx}(P_{yz} + \rho vw)\right) + 2P_{xz}P_{xy}}{\rho^2 c_{xx}^2} \\ \frac{-2\sqrt{3}\rho c_{xx}wP_{xz} + \rho^2 c_{xx}^2 w^2 + P_{zz}c_{xx}^2\rho + 2P_{xz}^2}{\rho^2 c_{xx}^2} \\ \frac{E_{rot}}{\rho} \end{bmatrix}, \mathbf{r_{c2}} = \begin{bmatrix} 0 \\ 0 \\ 1 \\ 0 \\ 0 \\ u - c_{xx} \\ 0 \\ \frac{2(vc_{xx}\rho - P_{xy})}{c_{xx}\rho} \\ \frac{wc_{xx}\rho - P_{xz}}{c_{xx}\rho} \\ 0 \\ 0 \end{bmatrix}, \mathbf{r_{c3}} = \begin{bmatrix} 0 \\ 0 \\ 0 \\ 1 \\ 0 \\ 0 \\ u - c_{xx} \\ 0 \\ \frac{(vc_{xx}\rho - P_{xy})}{c_{xx}\rho} \\ \frac{2(wc_{xx}\rho - P_{xz})}{c_{xx}\rho} \\ 0 \end{bmatrix},$$

$$\mathbf{r_{c4}} = \begin{bmatrix} 1 \\ u \\ v \\ w \\ u^2 \\ uv \\ uw \\ v^2 \\ vw \\ w^2 \\ 0 \end{bmatrix}, \mathbf{r_{c5}} = \begin{bmatrix} 0 \\ 0 \\ 0 \\ 0 \\ 0 \\ 0 \\ 0 \\ 1 \\ 0 \\ 0 \\ 0 \end{bmatrix}, \mathbf{r_{c6}} = \begin{bmatrix} 0 \\ 0 \\ 0 \\ 0 \\ 0 \\ 0 \\ 0 \\ 0 \\ 1 \\ 0 \\ 0 \end{bmatrix}, \mathbf{r_{c7}} = \begin{bmatrix} 0 \\ 0 \\ 0 \\ 0 \\ 0 \\ 0 \\ 0 \\ 0 \\ 0 \\ 1 \\ 0 \end{bmatrix}, \mathbf{r_{c8}} = \begin{bmatrix} 0 \\ 0 \\ 0 \\ 0 \\ 0 \\ 0 \\ 0 \\ 0 \\ 0 \\ 0 \\ 1 \end{bmatrix},$$

$$\mathbf{r_{c9}} = \begin{bmatrix} 0 \\ 0 \\ 0 \\ 1 \\ 0 \\ 0 \\ u + c_{xx} \\ 0 \\ \frac{(vc_{xx}\rho + P_{xy})}{c_{xx}\rho} \\ \frac{2(wc_{xx}\rho + P_{xz})}{c_{xx}\rho} \\ 0 \end{bmatrix}, \mathbf{r_{c10}} = \begin{bmatrix} 0 \\ 0 \\ 1 \\ 0 \\ 0 \\ u + c_{xx} \\ 0 \\ \frac{2(vc_{xx}\rho + P_{xy})}{c_{xx}\rho} \\ \frac{wc_{xx}\rho + P_{xz}}{c_{xx}\rho} \\ 0 \\ 0 \end{bmatrix}, \mathbf{r_{c11}} = \begin{bmatrix} 1 \\ u + \sqrt{3}c_{xx} \\ v + \frac{\sqrt{3}P_{xy}}{c_{xx}\rho} \\ w + \frac{\sqrt{3}P_{xz}}{c_{xx}\rho} \\ 3c_{xx}^2 + 2\sqrt{3}uc_{xx} + u^2 \\ \frac{\rho uvc_{xx} + u\sqrt{3}P_{xy} + \sqrt{3}c_{xx}^2\rho v + 3c_{xx}P_{xy}}{c_{xx}\rho} \\ \frac{\rho uwc_{xx} + u\sqrt{3}P_{xz} + \sqrt{3}c_{xx}^2\rho w + 3c_{xx}P_{xz}}{c_{xx}\rho} \\ \frac{\rho^2v^2c_{xx}^2 + 2\sqrt{3}P_{xy}c_{xx}\rho v + \rho c_{xx}^2P_{yy} + 2P_{xy}^2}{\rho^2c_{xx}^2} \\ \frac{c_{xx}\rho\left(\sqrt{3}(wP_{xy} + vP_{xz}) + c_{xx}(P_{yz} + \rho vw)\right) + 2P_{xz}P_{xy}}{\rho^2c_{xx}^2} \\ \frac{2\sqrt{3}\rho c_{xx}wP_{xz} + \rho^2c_{xx}^2w^2 + P_{zz}c_{xx}^2\rho + 2P_{xz}^2}{\rho^2c_{xx}^2} \\ \frac{E_{rot}}{\rho} \end{bmatrix}$$

The left eigenvectors, l_{pi}, can be interpreted as the strength of each wave, and when expressed in primitive variables are found to be

$$l_{p1} = \left[0, -\frac{\sqrt{3}\rho}{6c_{xx}}, 0, 0, \frac{1}{6c_{xx}^2}, 0, 0, 0, 0, 0, 0\right], \quad l_{p2} = \left[0, -\frac{P_{xy}}{2c_{xx}^2}, \frac{\rho}{2}, 0, \frac{P_{xy}}{2c_{xx}^3\rho}, -\frac{1}{2c_{xx}}, 0, 0, 0, 0, 0\right],$$

$$l_{p3} = \left[0, -\frac{P_{xz}}{2c_{xx}^2}, 0, \frac{\rho}{2}, \frac{P_{xz}}{2c_{xx}^3\rho}, 0, -\frac{1}{2c_{xx}}, 0, 0, 0, 0\right],$$

$$l_{p4} = \left[1, 0, 0, 0, -\frac{1}{3c_{xx}^2}, 0, 0, 0, 0, 0, 0\right], \quad l_{p5} = \left[0, 0, 0, 0, \frac{4P_{xy}^2 - \rho c_{xx}^2P_{yy}}{3\rho^2c_{xx}^4}, -\frac{2P_{xy}}{c_{xx}^2\rho}, 0, 1, 0, 0, 0\right],$$

$$l_{p6} = \left[0, 0, 0, 0, \frac{4P_{xz}P_{xy} - \rho c_{xx}^2P_{yz}}{3\rho^2c_{xx}^4}, -\frac{P_{xz}}{c_{xx}^2\rho}, -\frac{P_{xy}}{c_{xx}^2\rho}, 0, 1, 0, 0\right],$$

$$l_{p7} = \left[0, 0, 0, 0, \frac{4P_{xz}^2 - \rho c_{xx}^2P_{zz}}{3\rho^2c_{xx}^4}, 0, -\frac{2P_{xz}}{c_{xx}^2\rho}, 0, 0, 1, 0\right], \quad l_{p8} = \left[0, 0, 0, 0, -\frac{E_{rot}}{3\rho c_{xx}^2}, 0, 0, 0, 0, 0, 1\right]$$

$$l_{p9} = \left[0, -\frac{P_{xz}}{2c_{xx}^2}, 0, \frac{\rho}{2}, -\frac{P_{xz}}{2c_{xx}^3\rho}, 0, \frac{1}{2c_{xx}}, 0, 0, 0, 0\right],$$

$$l_{p10} = \left[0, -\frac{P_{xy}}{2c_{xx}^2}, \frac{\rho}{2}, 0, -\frac{P_{xy}}{2c_{xx}^3\rho}, \frac{1}{2c_{xx}}, 0, 0, 0, 0, 0\right], \quad l_{p11} = \left[0, \frac{\sqrt{3}\rho}{6c_{xx}}, 0, 0, \frac{1}{6c_{xx}^2}, 0, 0, 0, 0, 0, 0\right]$$

Provided that P_{xx} and ρ remain real and greater than zero, this system of equations has real eigenvalues and a complete linearly independent set of eigenvectors and is therefore strictly hyperbolic. This condition holds in any Cartesian reference frame, as the x-direction used for the analysis above was chosen quite arbitrarily. Returning to the assumed form of the non-equilibrium distribution function for the Gaussian closure, the condition of hyperbolicity is maintained when $\rho > 0$ and the symmetric tensor Θ_{ij} is positive definite.

III. Parallel Implicit AMR Upwind Finite-Volume Scheme

A. Finite-Volume Discretization

The preceding moment equations for the Gaussian closure are solved herein by applying an upwind finite-volume method in which the conservation equations are integrated over hexahedral cells of a body-fitted, multi-block mesh. The finite-volume formulation applied to cell (i, j, k) can be expressed as

$$\frac{\mathrm{d}\mathbf{U}_{i,j,k}}{\mathrm{d}t} = -\frac{1}{V_{i,j,k}} \sum_{m} \left(\vec{\mathbf{F}} \cdot \vec{n}\, \Delta A \right)_{i,j,k.m} + \mathbf{S}_{i,j.k} = \mathbf{R}_{i,j,k}(\mathbf{U}) \,, \tag{20}$$

where $\mathbf{U}$ is the vector of conserved solution variables, $\vec{\mathbf{F}} = (\mathbf{E}, \mathbf{F}, \mathbf{G})$ is the hyperbolic solution flux dyad, $\mathbf{S}$ is the source term associated with the collisional processes, $V_{i,j,k}$ is the volume of cell (i, j, k), and ΔA and $\vec{n}$ are the area and unit outward normal vector of the cell face m respectively and $\mathbf{R}_{i,j,k}(\mathbf{U})$ is the residual vector. The numerical fluxes at the faces of each cell are determined using the least-squares piecewise limited linear solution reconstruction procedure of Barth[21] and Riemann solver based flux functions. The limiter of Venkatakrishnan[22] and an extension of the approximate linearised Riemann solver of Roe[23] for the Gaussian moment equations are both used.

B. Parallel Adaptive Mesh Refinement

The spatial discretisation procedure described above allows for solution-directed block-based AMR and an efficient and highly scalable parallel implementation has been achieved via domain decomposition.[12–14, 24] In particular, a flexible block-based hierarchical octree data structure has been developed and is used to facilitate automatic solution-directed mesh adaptation on a multi-block body-fitted hexahedral mesh according to physics-based refinement criteria. Local refinement and coarsening of the mesh is carried out by division and merging of solution blocks, respectively. A domain decomposition procedure is used where the solution blocks making up the computational mesh are distributed equally among available processors, with more than one block permitted per processor. A Morton ordering space filling curve is used to provide nearest-neighbour ordering of the solution blocks in the multi-block hexahedral AMR mesh for more efficient load balancing.[25] Refer to the recent papers by Northrup and Groth[24] and Gao and Groth[12, 14] for further details of the parallel AMR scheme.

C. Solution of Semi-Discrete Form of Moment Equations

1. Point-Implicit Time Marching Method for Unsteady Flows

As the relaxation times, τ_t and τ_r, become very small under near-equilibrium conditions, the numerical stiffness of the system increases. To handle these difficulties, a point-implicit finite-volume formulation with second-order semi-implicit time-marching is used to integrate the set of differential equations that results from the spatial discretisation for time-varying flow problems. The hyperbolic fluxes at cell boundaries are evaluated using Riemann-solver based flux functions (Roe's scheme is used for the solved flow problems described in this study, though other approximate solvers such as the Harten-van Leer-Lax-Einfeldt (HLLE) have been implemented and are equally functional). A semi-implicit time marching method is used to evolve the solution forward in time in which an implicit scheme is applied to the source terms of the equations, while an explicit scheme is used in the flux evaluations. Originally developed and described by McDonald and Groth[8–10] for two-dimensional flow problems using the Gaussian closure, this method has been extended into three dimensions and is used to evaluate the effectiveness of the Gaussian closure for various flow regimes, and also serves as a baseline with which accelerated solution techniques can be compared to.

2. Newton's Method for Steady-State Flows

Alternate accelerated solution methods have also been examined herein to enhance the performance and efficiency of obtainingsolutions to the semi-discrete form of the Gaussian moment equations for steady-state time-invariant flows. As noted above, the semi-discrete form of the governing equations given in Equation (20) form a coupled set of non-linear ordinary differential equations. However, steady-state solutions (the primary focus here), can be computed directly here by solving the nonlinear algebraic equations represented by $\mathbf{R}(\mathbf{U}) = 0$ using Newton's method. Given an estimate to the solution to $\mathbf{R}(\mathbf{U}) = 0$ at iteration level n,

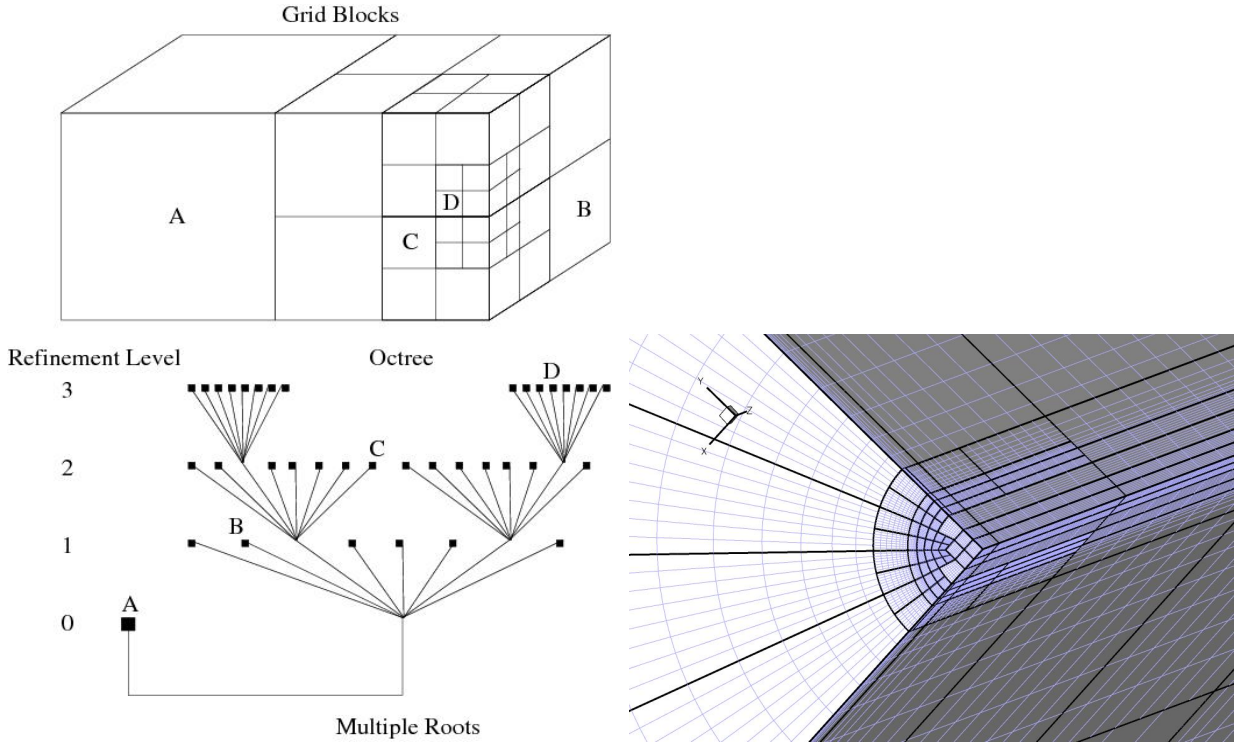

Figure 1. (a) Octree data structure and block connectivity for an AMR multi-block hexahedral mesh, (b) Sample 3D AMR for multiblock body-fitted hexahedral mesh for internal flow of a fuel line.

the following system of linear equations can be solved in Newton's method to obtain an improved estimate for the solution at the $n+1$ iteration level, $\mathbf{U}^{(n+1)}$, satisfying $\Delta\mathbf{U}^{(n+1)} = \mathbf{U}^{(n+1)} - \mathbf{U}^{(n)}$:

$$\left(\frac{\partial \mathbf{R}}{\partial \mathbf{U}}\right)^{n+1} \Delta\mathbf{U}^{n+1} = \mathbf{J}\Delta\mathbf{U}^{n+1} \approx -\mathbf{R}\left(\mathbf{U}^{n+1}\right) \tag{21}$$

Given an initial estimate for the steady-state solution, $\mathbf{U}^0$, successively improved estimates for the solution $\mathbf{U}^{n+1}$ are obtained by solving Equation (21) at each step, n, of the Newton method, where $\mathbf{J} = \frac{\partial \mathbf{R}}{\partial \mathbf{U}}$ is the residual Jacobian. The iterative procedure is repeated until an appropriate norm of the solution residual is sufficiently small, i.e., $||\mathbf{R}(\mathbf{U}^{(n+1)})||_2 < \epsilon||\mathbf{R}(\mathbf{U}^{(n)})||_2$ where ϵ is some small parameter (typically, $\epsilon \approx 10^{-7}$–10^{-11}).

Each step of Newton's method requires the solution of a system of linear equations of the form $\mathbf{Jx} = \mathbf{b}$. This system is large, sparse, and non-symmetric and a preconditioned GMRES method[26,27] is used for its solution. In particular, a restarted version of the GMRES algorithm, GMRES(m), is used, where m is the number of steps after which the GMRES algorithm is restarted. Application of this iterative technique leads to an overall solution algorithm with iterations within iterations: the "inner loop" iterations involving the solution of the linear system and the "outer loop" iterations associated with the solution of the nonlinear problem. An inexact Newton method is adopted here in which the inner iterations are not fully converged at each Newton step. The inner iterations are carried out only until $||\mathbf{R} + \mathbf{J}\Delta\mathbf{U}||_2 \leq \zeta||\mathbf{R}||_2$, where ζ is typically in the range 0.01–0.5. As discussed by Dembo *et al.*,[28] an exact solution of the linear system is not necessary for rapid convergence of Newton's method.

Preconditioning is required for the linear solver to be effective. Right preconditioning of the form $(\mathbf{JM}^{-1})(\mathbf{Mx}) = \mathbf{b}$ is used here where $\mathbf{M}$ is the preconditioning matrix. An additive Schwarz global preconditioner with variable overlap[27,29,30] is used in conjunction with local preconditioners based on a block ILU(f) or BILU(f) factorization of an approximate Jacobian for each subdomain. Here, f is the level of fill. This combination of preconditioning fits well with the block-based AMR described by Northrup and

Groth[31] and is compatible with domain decomposition methods, readily enabling parallel implementation of the overall Newton method. Rather efficient parallel implementations of implicit algorithms via Schwarz preconditioning have been developed by Keyes and co-researchers and successfully applied to the prediction of transonic full potential, low-Mach-number compressible combusting, and three-dimensional inviscid flows.[29,32,33]

As the GMRES algorithm does not explicitly require the evaluation of the global Jacobian matrix, $\mathbf{J}$, a so-called "matrix-free" or "Jacobian-free" approach can be adopted and is used here. Numerical differentiation based on Fréchet derivatives is used to approximate the matrix-vector product $\mathbf{J}\mathbf{M}^{-1}\mathbf{x}$ as follows:

$$\mathbf{J}\mathbf{M}^{-1}\mathbf{x} \approx \frac{\mathbf{R}(\mathbf{U} + \varepsilon\mathbf{M}^{-1}\mathbf{x}) - \mathbf{R}(\mathbf{U})}{\varepsilon}, \tag{22}$$

where $\mathbf{R}(\mathbf{U} + \varepsilon\mathbf{M}^{-1}\mathbf{x})$ is the residual vector evaluated at some perturbed solution state and ε is a small scalar quantity. Although the performance of the Jacobian-free method is sensitive to the choice of ε, Neilsen *et al.*[34] have found that $\varepsilon = \varepsilon_\circ / ||\mathbf{x}||_2^{1/2}$ seems to work well, with $\varepsilon_\circ \approx 10^{-8}$–$10^{-7}$.

IV. Numerical Results and Validation

The Gaussian closure is applied here to various flow problems to demonstrate its ability to model commonly-encountered flow phenomena, including drag, boundary layer evolution, and slip flow modelling. For the most part, the continuum and non-equilibrium flow problems considered here are based on three-dimensional extensions of the two-dimensional cases considered in the previous studies of McDonald and Groth.[8–10,35] The solid-wall boundary conditions derived by McDonald and Groth[8–10] and described briefly in Section 3 are used exclusively here.

A. Couette Flow

One of the main characteristics of increasing Knudsen number is the appearance of slip flows at solid walls. In the continuum regime, particle density at the wall is sufficiently high that a large number of particles will collide with the wall and undergo a change in velocity corresponding to the velocity of the wall. With increasingly rarefied flows, fewer particles will collide with the wall and undergo this velocity change, resulting in a decrease in macroscopic fluid velocity measurements at the wall. This disparity between the velocity of the wall and the velocity of the flow at the wall begins at a Knudsen number range of about $0.01 < \mathrm{Kn} < 0.1$. Accommodating slip flows in continuum flows usually involves incorporating complex boundary conditions as an extension to the continuum-based equations.[36] The Gaussian closure however, requires no case-specific boundary conditions beyond those already used for specifying solid-wall boundary conditions, as slip flow effects fall out naturally from the equation set. This becomes a powerful tool for modelling flows that lie in the continuum-slip flow regimes, as additional computational resources do not need to be allocated for varying boundary conditions.

Planar Couette flow is studied here to illustrate the Gaussian closure's ability to model boundary layer and shear stress evolution in various flow regimes. For this particular problem, the two plates move at 30 m/s in opposite directions in argon at 288 K in standard pressure, and the setup is extended in the z direction. The solution of the Gaussian closure was used with periodic boundary conditions were used at the inflow and outflow boundaries, while the solid wall boundaries described in Section 3 are used for the two plates. The mesh resolution with three levels of mesh refinement were used for this problem, generating a total of 43,200 cells. As the problem is relatively simple and the flow is almost one-dimensional, the use of AMR was not absolutely necessary to reach a steady solution within a reasonable amount of time. A CFL number of 0.5 was implemented, while solution residuals were run to 4×10^{-6} at which point the shear stress and slip velocity were not observed to undergo significant changes.

Figure 2(a) shows the non-dimensionalised velocity $\frac{u}{U}$, where u is the fluid velocity at the wall and U is the wall velocity, versus the Knudsen number based on the separation of the two plates. The continuum solution using the Navier-Stokes equations with no extra treatment for slip flows calculates the fluid velocity at the wall to be equal to the velocity of the wall regardless of Knudsen number. The free molecular solution generates an infinite slip velocity at the wall, with the fluid velocity at the wall equal to zero for all flows. Lees solution (1959)[37] provides an analytical solution to this problem that predicts the slip velocity and shear stress at the wall, gradually transitioning from the continuum result to the free-molecular. The Gaussian

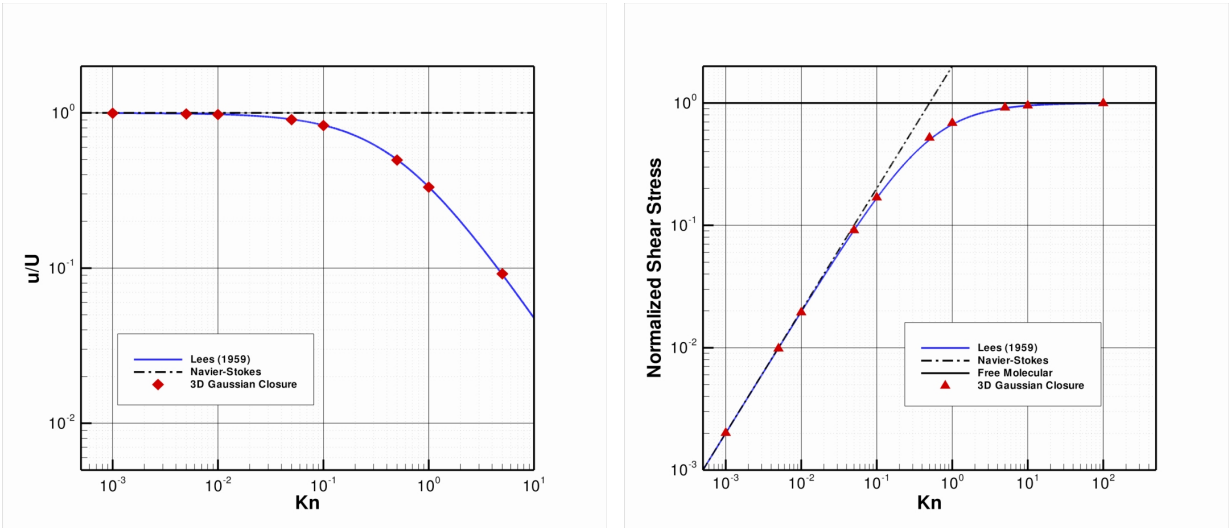

(a) (b)

Figure 2. (a) Normalised fluid velocity at the wall vs. Knudsen number. Note that the free-molecular solution gives $u = 0$ at the wall regardless of Knudsen number, (b) Normalised shear stress at the wall vs. Knudsen number.

solution is capable of modelling the formation of a slip velocity and follows Lees solution closely for a wide range of Knudsen numbers.

The shear pressure profile for the same problem can be seen in Figure 2(b). For comparison purposes, the shear stresses are normalised to the free molecular solution as $\frac{\tau_{xy}}{\rho U \sqrt{\frac{2kT}{\pi m}}}$. Use of the continuum formulation predicts an ever-increasing shear stress with increasing Knudsen number, while the free-molecular shear stress remains constant regardless of Knudsen number. The Gaussian solution predicts a smooth transition between the continuum and free-molecular solutions and is in very close agreement with the analytical solution by Lees.

B. Flat Plate Boundary Layer Flow

The Gaussian closure's ability to model slip flows and its effect on the boundary layer is further demonstrated here through the prediction of boundary layer development over a flat plate. Free stream conditions for this flow consist of air at 288 K flowing at a Mach number of 0.2 under standard atmospheric pressure. The Knudsen number is varied by sampling the boundary layer profile along different lengths along the plate downstream from the leading edge. The continuum boundary layer profile at $\mathrm{Kn} = 4.5 \times 10^{-5}$ was sampled at 1.5×10^{-3} m, while the transition regime boundary layer profile at $\mathrm{Kn} = 2.6 \times 10^{-1}$ was sampled at 2.6×10^{-7} m. The associated Reynolds number for the continuum and transition regime flows are $\mathrm{Re} = 6505$ and $\mathrm{Re} = 1.1$ respectively, well within the laminar flow regime. Solutions of the Gaussian closure for the corresponding problem in two dimensions were obtained by McDonald and Groth[8–10,35] used AMR with ten levels of refinement resulting in a very high mesh resolution at the surface of the flat plate. For the Gaussian closure solutions in three-dimensions, this level of mesh refinement proved to be too costly and only four levels of refinement were used, resulting in a total of 250,000 cells. The mesh is linearly varying in space such that a higher resolution is achieved closer to the plate surface. Solid wall boundary conditions were again employed for the plate, with a far field situated 10 plate lengths above the plate and inflow and outflow boundary conditions situated upstream and downstream from the plate, respectively. A CFL number of 0.6 was used with a solution residual of 1×10^{-5} . Solution convergence was found to be very slow at this point owing to the explicit nature of the time marching scheme, but the boundary layer was found to have been developed sufficiently for a good comparison with the classical Blasius solution.[38]

Figure 3 compares the boundary layer profiles between the Knudsen number-independent Blasius solution[38] and solutions from the continuous ($\mathrm{Kn} = 4.5 \times 10^{-5}$) and transition regimes ($\mathrm{Kn} = 2.6 \times 10^{-1}$). Blasius

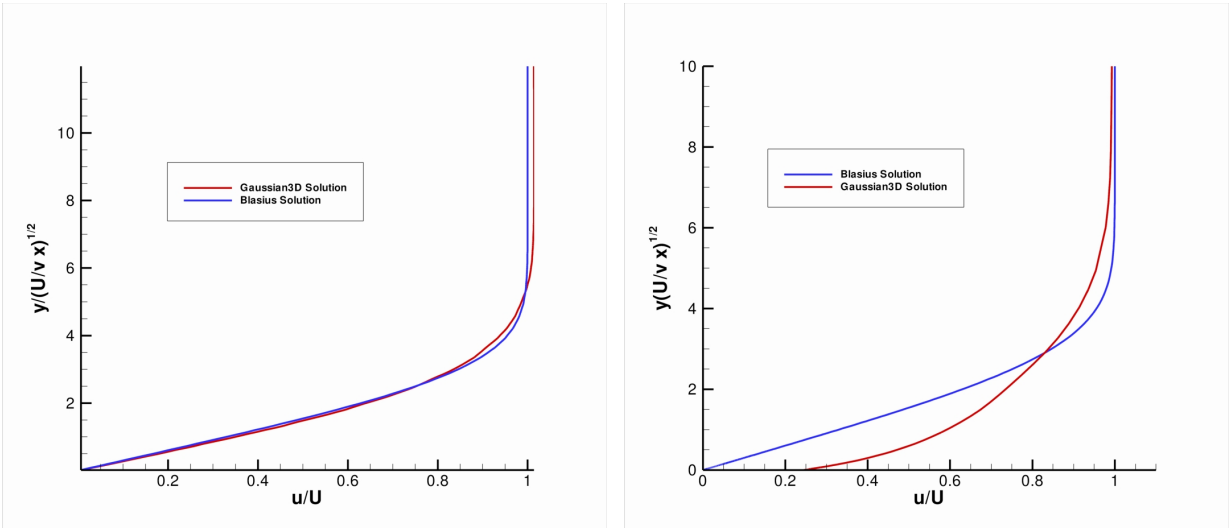

(a) (b)

Figure 3. Flat plate normalised velocity distribution in developing boundary layer at varying Knudsen numbers (a) Continuum Regime, $\mathrm{Kn} = 4.5 \times 10^{-5}$**, (b) Transition Regime,** $\mathrm{Kn} = 2.6 \times 10^{-1}$**.**

proposed a relation between a non-dimensionalised velocity u/U normalised to the free stream velocity U, and a non-dimensional number $y\sqrt{\frac{U}{\nu x}}$ relating to the development of the boundary layer at a certain position above the plate. These non-dimensionalised numbers are calculated for both the continuous and transitional case for comparison purposes.

From Figure 3, it is quite evident that the continuum result matches closely with the Blasius approximation with a zero slip velocity at the wall, while the transitional regime solution clearly shows a non-zero velocity at the wall. Calculations were performed with approximately 100 cells lying within the boundary layer. While the solution can be obtained both with and without AMR, the isotropic nature of the AMR algorithm generates many blocks in the extruded direction of the plate. The gradients in this direction are negligible, but the additional blocks substantially increase the memory requirements for the model leading to longer computational and post-processing times. The equation set however, remains equally capable in resolving the slip flow phenomena exhibited with increasing Knudsen numbers and give credence to the Gaussian closure technique.

C. Flow Past an Immersed Cylinder

The drag forces exerted on a cylinder in an immersed flow is a well studied topic in aerodynamics and serves as an excellent platform here with which to evaluate the validity and accuracy of the Gaussian closure. The effects of laminar flow past a cylinder in both the continuum and transitional regimes has been studied experimentally by Coudeville *et al.*,[39] with focus on the drag coefficient with both varying Reynolds and Knudsen numbers. Approximate solutions to the cylinder drag in the continuum and transitional regime have also been put forward by Patterson.[40] For the flow problem considered here, the cylinder radii varies from 3.36×10^{-5} to 3.36×10^{-9} m, corresponding to a Knudsen number ranging from $\mathrm{Kn} = 1 \times 10^{-3}$ to $\mathrm{Kn} = 10$. The computed Gaussian closure solutions are for air at 288 K at standard atmospheric pressure. Two speed ratios of $S = 0.107$ and $S = 0.027$ corresponding to a Mach number of $\mathrm{Ma} = 0.128$ and $\mathrm{Ma} = 0.032$ are used for setting the free stream velocity, where the speed ratio is defined as the ratio between the bulk speed of the fluid to the most probable random speed of a particle, and is proportional to the Mach number. The Reynolds number for these flows ranges from $\mathrm{Re} = 0.005$ to $\mathrm{Re} = 188$.

A sample three-dimensional grid block layout with AMR implemented for this immersed cylinder flow is shown in Figure 5. Solid wall boundary conditions were used for the surface of the cylinder, with the far field set at 100 times the cylinder radius. However, for $\mathrm{Kn} = 1 \times 10^{-1}$, the boundary layer formed around the cylinder expands considerably, and the far field boundaries were extended up to 400 times the cylinder

radius to avoid any interaction with the boundary layer. Mesh resolution at the surface of the cylinder were set to similar values as those of McDonald and Groth,[8–10,35] with a final three-dimensional mesh resolution ranging from 37,000 to 67,000 cells. As in a similar case with the previous flat plate problem, the mesh is stretched to create a higher concentration of cells near the cylinder surface. The Gaussian closure was solved with a CFL number of 0.5, with a solution residual of 1×10^{-5} at which point the calculated drag coefficient was not observed to vary significantly and were in good agreement with the values computed by McDonald and Groth.[8–10,35]

The drag coefficient is plotted against the Knudsen number in Figure 4 for two different speed ratios S. The Gaussian closure is successful in duplicating the experimental results of Coudeville in both the continuum and transition regimes. However, the closure solution begins to over-predict the drag coefficient compared to both the experimental results and the theoretical solutions when the fluid begins to transition into the free molecular flow regime at about $\mathrm{Kn} > 5 \times 10^{-1}$. While the Gaussian method tends to over-predict the drag coefficient in this region possibly due to the neglected heat transfer effects, it is successful in demonstrating a smooth transition of drag coefficients while moving from the continuum regime into the free molecular regime.

It should be noted that as the Knudsen number drops and the flow approaches the free molecular regime, the flow structure also changes dramatically. Figure 6 shows the velocity profiles for the flow around the cylinder in the continuum regime ($\mathrm{Kn} = 1 \times 10^{-3}$) through the transitional regime ($\mathrm{Kn} = 1 \times 10^{-1}$), right up to the boundary of the free molecular regime ($\mathrm{Kn} = 1$). A clear separation of the flow with a recirculation area in the wake of the cylinder can be seen in the continuum result which agrees with standard experimental results for this type of flow. As the Knudsen number is increased, the thickness of the boundary layer increases and the flow remains attached. This increase in boundary layer thickness disturbs the far field flow much more prominently, and numerical results for these higher Knudsen numbers required a larger domain to accommodate their effects. The increase in boundary layer thickness is in line with basic kinetic theory for rarefied flows, as the reduction in interparticle collisions comes about from larger mean free paths. The use of AMR drastically reduces the overall computational cost for these models while still maintaining a high resolution in areas of interest on the surface of the cylinder and in the downstream regions.

D. Parallel NKS Performance

The NKS algorithm described in Section 2 has been applied towards the solution of the flow problems mentioned above and shows great promise in providing accelerated steady state solutions while maintaining the solution characteristics of the Gaussian closure. To illustrate the effectiveness of the NKS algorithm, the residual reduction per iteration for an immersed cylinder flow in the continuum regime is shown below in Figure 7(a). Note that while each iteration of Newton's method requires more resources than a simple time step in the semi-implicit time marching scheme due to the internal GMRES iterations, the total number of NKS iterations required to drive the residual to similar levels is drastically reduced, as can be seen in Figure 7(b). With a simple 8-block cylinder geometry with no AMR running on eight Intel(R) Core(TM) i7 CPUs at 3.33Ghz each, typical computation times for the NKS solution scheme range from 20-25 minutes, whereas the semi-implicit time marching scheme requires 20 hours. While significant challenges still remain in optimizing the proposed NKS method for solution of the Gaussian closure, the results obtained herein are certainly very promising and future research will involve further optimization of the Newton method for a wider range of problems.

V. Conclusion

The Gaussian closure in combination with a parallel, implicit, AMR, upwind, finite-volume scheme has been considered herein as an alternative for the simulation of micro-scale transition regime flows. The mathematical derivation of a set of strictly hyperbolic system of PDEs opens the door for physically accurate yet computationally inexpensive algorithms in place of extensive modifications to the continuum-based Navier-Stokes equations. The relatively simple application of the parallel implicit NKS scheme for accelerated steady-state and time-accurate solutions is another advantage for the Gaussian closure for micron-scale flows. While the equation set as is does not take into account the effects of heat transfer, flow behaviour expected in the flow regimes for the cases studied here are accurately predicted. Future work will involve extending the equation set to include heat transfer terms, and an examination of the suitability of the Gaussian

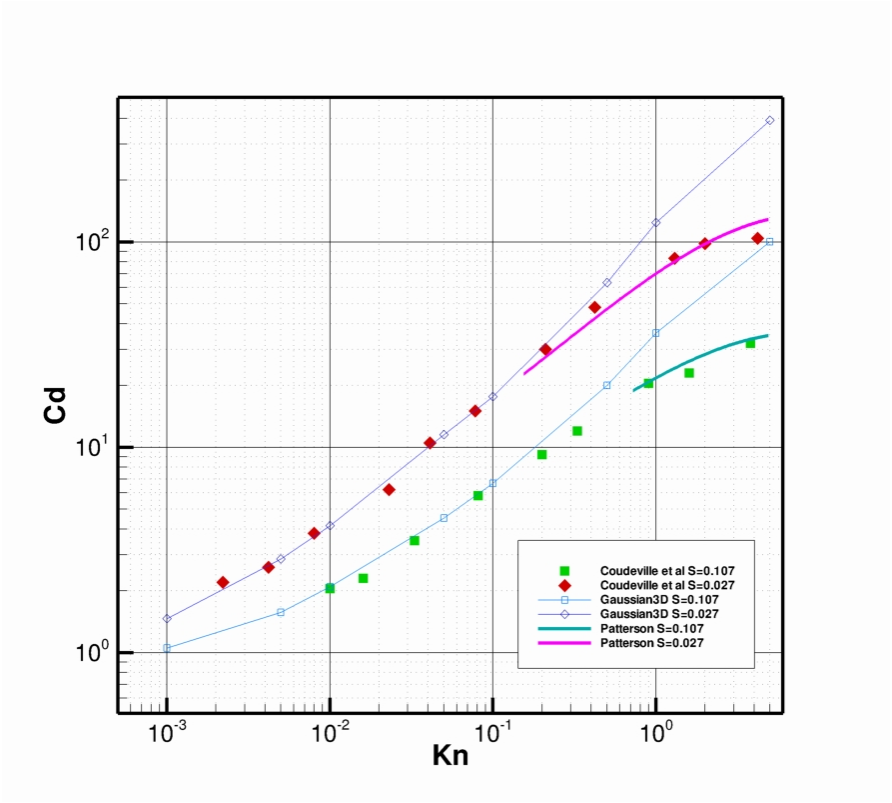

Figure 4. Drag coefficient for varying Knudsen numbers at two speed ratios: Gaussian closure vs. experimental results.

closure for other classes of non-equilibrium flows.

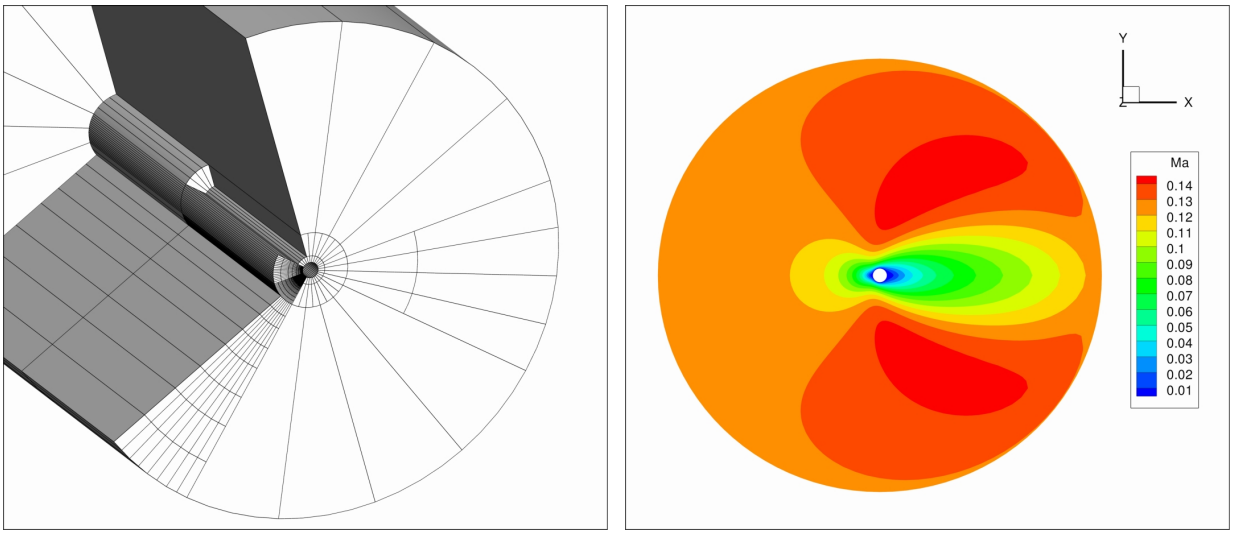

(a) (b)

Figure 5. (a) A cutaway view of the radial mesh blocks created by the AMR algorithm for immersed cylinder flow, showing refined block structure at the surface of the cylinder and in the downstream regions. Mesh sizes are also shown in the lower left blocks. (b) Sample result of Mach number profile for $\mathrm{Kn} = 1 \times 10^{-1}$**.**

References

[1]Bird, G. A., *Molecular Gas Dynamics and the Direct Simulation of Gas Flows*, Clarendon Press, Oxford, 1994.

[2]Maxwell, J. C., "On the Dynamical Theory of Gases," *Philosophical Transactions of the Royal Society of London*, Vol. 157, 1867, pp. 49–88.

[3]Boltzmann, L., "Weitere Studien über das Wärmegleichgewicht unter Gasmolekülen," *Sitz. Math.-Naturwiss. Cl. Akad. Wiss. Wien*, Vol. 66, 1872, pp. 275–370.

[4]Grad, H., "On the Kinetic Theory of Rarefied Gases," *Communications on Pure and Applied Mathematics*, Vol. 2, 1949, pp. 331–407.

[5]Levermore, C. D., "Moment Closure Hierarchies for Kinetic Theories," *Journal of Statistical Physics*, Vol. 83, 1996, pp. 1021–1065.

[6]Junk, M., "Domain of Definition of Levermore s Five-Moment System," *Journal of Statistical Physics*, Vol. 93, No. 5/6, 1998, pp. 1143–1167.

[7]Godunov, S. K., "Finite-Difference Method for Numerical Computations of Discontinuous Solutions of the Equations of Fluid Dynamics," *Matematicheskii Sbornik*, Vol. 47, 1959, pp. 271–306.

[8]McDonald, J. and Groth, C. P. T., "Numerical Modeling of Micron-Scale Flows Using the Gaussian Moment Closure," Paper 2005-5035, AIAA, June 2005.

[9]McDonald, J. and Groth, C. P. T., "Extended Fluid-Dynamic Model for Micron-Scale Flows Based on Gaussian Moment Closure," Paper 2008-691, AIAA, January 2008.

[10]Groth, C. P. T. and McDonald, J. G., "Towards Physically-Realizable and Hyperbolic Moment Closures for Kinetic Theory," *Continuum Mechanics and Thermodynamics*, Vol. 21, 2010, pp. 467–493.

[11]Hittinger, J. A., *Foundations for the Generalization of the Godunov Method to Hyperbolic Systems with Stiff Relaxation Source Terms*, Ph.D. thesis, University of Michigan, 2000.

[12]Gao, X. and Groth, C. P. T., "Parallel Adaptive Mesh Refinement Scheme for Three-Dimensional Turbulent Non-Premixed Combustion," Paper 2008-1017, AIAA, January 2008.

[13]Gao, X., *A Parallel Solution-Adaptive Method for Turbulent Non-Premixed Combusting Flows*, Ph.D. thesis, University of Toronto, August 2008.

[14]Gao, X. and Groth, C. P. T., "A Parallel Solution-Adaptive Method for Three-Dimensional Turbulent Non-Premixed Combusting Flows," *Journal of Computational Physics*, Vol. 229, No. 5, 2010, pp. 3250–3275.

[15]Groth, C. P. T. and Northrup, S. A., "Parallel Implicit Adaptive Mesh Refinement Scheme for Body-Fitted Multi-Block Mesh," Paper 2005-5333, AIAA, June 2005.

[16]Northrup, S. A. and Groth, C. P. T., "Solution of Laminar Combusting Flows Using a Parallel Implicit Adaptive Mesh Refinement Algorithm," submitted for presentation at the Fourth International Conference on Computational Fluid Dynamics, Ghent, Belgium, July 10–14, 2006, February 2006.

[17]Northrup, S. A. and Groth, C. P. T., "Prediction of Unsteady Laminar Flames Using a Parallel Implicit Adaptive Mesh Refinement Algorithm," *Proceedings of the U. S. National Combustion Meeting, Ann Arbor, Michigan, U.S.A., May 17–20, 2009*, 2009, p. paper 23H3.

[18]Gombosi, T. I., *Gaskinetic Theory*, Cambridge University Press, Cambridge, 1994.

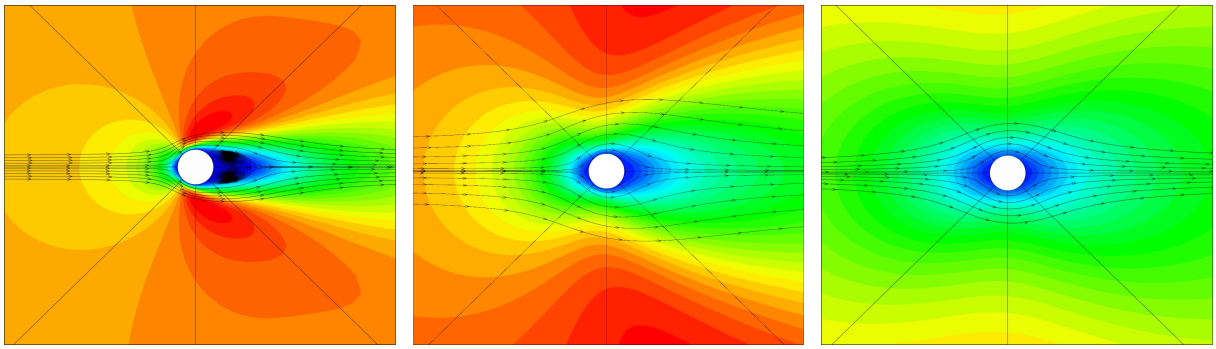

(a) (b) (c)

Figure 6. Comparison of x-directional velocity profile for immersed cylinder flow for various Knudsen numbers (a) $Kn = 1 \times 10^{-3}$**, (b)** $Kn = 1 \times 10^{-1}$**, (c)** $Kn = 1$.

[19]Bhatnagar, P. L., Gross, E. P., and Krook, M., "A Model for Collision Processes in Gases. I. Small Amplitude Processes in Charged and Neutral One-Component Systems," *Physical Review*, Vol. 94, No. 3, 1954, pp. 511–525.

[20]Bird, G. A., *Molecular Gas Dynamics*, Clarendon Press, Oxford, 1976.

[21]Barth, T. J., "Recent Developments in High Order K-Exact Reconstruction on Unstructured Meshes," Paper 93-0668, AIAA, January 1993.

[22]Venkatakrishnan, V., "On the Accuracy of Limiters and Convergence to Steady State Solutions," Paper 93-0880, AIAA, January 1993.

[23]Roe, P. L., "Approximate Riemann Solvers, Parameter Vectors, and Difference Schemes," *Journal of Computational Physics*, Vol. 43, 1981, pp. 357–372.

[24]Northrup, S. A. and Groth, C. P. T., "Solution of Laminar Diffusion Flames Using a Parallel Adaptive Mesh Refinement Algorithm," Paper 2005-0547, AIAA, January 2005.

[25]Aftosmis, M. J., Berger, M. J., and Murman, S. M., "Applications of Space-Filling Curves to Cartesian Methods for CFD," Paper 2004-1232, AIAA, January 2004.

[26]Saad, Y. and Schultz, M. H., "GMRES: A Generalized Minimal Residual Algorithm for Solving Nonsymmetric Linear Equations," *SIAM Journal for Scientific and Statistical Computing*, Vol. 7, No. 3, 1986, pp. 856–869.

[27]Saad, Y., *Iterative Methods for Sparse Linear Systems*, PWS Publishing Company, Boston, 1996.

[28]Dembo, R. S., Eisenstat, S. C., and Steihaug, T., "Inexact Newton Methods," *SIAM Journal on Numerical Analysis*, Vol. 19, No. 2, 1982, pp. 400–408.

[29]Gropp, W. D., Kaushik, D. K., Keyes, D. E., and Smith, B. F., "High-Performance Parallel Implicit CFD," *Parallel Computing*, Vol. 27, 2001, pp. 337–362.

[30]Knoll, D. A. and Keyes, D. E., "Jacobian-Free Newton-Krylov Methods: A Survey of Approaches and Applications," *Journal of Computational Physics*, Vol. 193, 2004, pp. 357–397.

[31]Northrup, S. A. and Groth, C. P. T., "Parallel Implicit Adaptive Mesh Refinement Algorithm for Solution of Laminar Combusting Flows," for presentation at the 14th Annual Conference of the CFD Society of Canada, Kingston, Ontario, Canada, July 16–18, 2006, February 2006.

[32]Knoll, D. A., McHugh, P. R., and Keyes, D. E., "Newton-Krylov Methods for Low-Mach-Number Compressible Combustion," *AIAA Journal*, Vol. 34, No. 5, 1996, pp. 961–967.

[33]Cai, X.-C., Gropp, W. D., Keyes, D. E., Melvin, R. G., and Young, D. P., "Parallel Newton-Krylov-Schwarz Algorithms for the Transonic Full Potential Equations," *SIAM Journal on Scientific Computing*, Vol. 19, No. 1, 1998, pp. 246–265.

[34]Nielsen, E. J., Anderson, W. K., Walters, R. W., and Keyes, D. E., "Application of Newton-Krylov Methodology to a Three-Dimensional Unstructured Euler Code," Paper 95-1733-CP, AIAA, June 1995.

[35]McDonald, J., *Extended Fluid-Dynamic Modelling for Numerical Solution of Micro-Scale Flows*, Ph.D. thesis, University of Toronto, October 2010.

[36]Zhang, T., Jia, L., and Wang, Z., "Validation of Navier-Stokes equations for slip flow analysis within transition region," *International Journal of Heat and Mass Transfer*, Vol. 51, No. 25-26, 2008, pp. 6323–6327.

[37]Vincenti, W. G. and Kruger, C. H., *Introduction to Physical Gas Dynamics*, R. E. Krieger Publishing, Huntington, NY, 1975.

[38]Granger, R. A., *Fluid Mechanics*, Dover, New York, 1995.

[39]Coudeville, P. T. H. and Brun, E., "Drag Measurements in Slip and Transition Flow," *Proceedings of the Fourth International Symposium on Rarefied Gas Dynamics*, Academic Press, New York, 1965, pp. 444–467.

[40]Patterson, G. N., *Introduction to the Kinetic Theory of Gas Flows*, University of Toronto Press, Toronto, 1961.

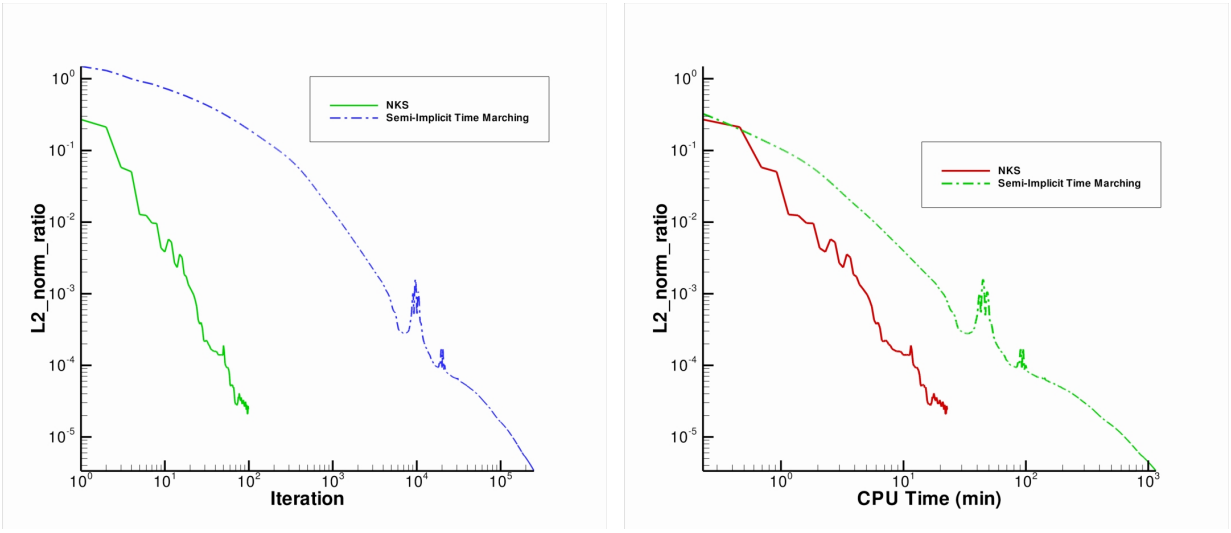

(a) (b)

Figure 7. Comparison of L2-norm ratios for the semi-implicit time marching and NKS computations for flow past an immersed cylinder in the continuum regime ($Kn = 0.001$), with convergence plotted as a function of (a) iteration and (b) total CPU time.